Nanoscale

ARTICLE

Real-time measurement of the intracellular pH of yeast cells during glucose metabolism using ratiometric fluorescent nanosensors‡

Received 00th January 20xx,
Accepted 00th January 20xx

DOI: 10.1039/c7nr00906b

www.rsc.org/

Mohamed M Elsutohy, †[a] Veeren M Chauhan, †[a] Robert Markus, [b] Mohammed Aref Kyyaly, [c,d] Saul JB Tendler [a,e] and Jonathan W Aylott*[a]

Intracellular pH is a key parameter that influences many biochemical and metabolic pathways that can also be used as an indirect marker to monitor metabolic and intracellular processes. Herein, we utilise ratiometric fluorescent pH-sensitive nanosensors with an extended dynamic pH range to measure the intracellular pH of yeast (*Saccharomyces cerevisiae*) during glucose metabolism in real-time. Ratiometric fluorescent pH-sensitive nanosensors consisting of a polyacrylamide nanoparticle matrix covalently linked to two pH-sensitive fluorophores, Oregon green (OG) and 5(6)carboxyfluorescein (FAM), and a reference pH-insensitive fluorophore, 5(6)carboxytetramethylrhodamine (TAMRA), were synthesised. Nanosensors were functionalised with acrylamidopropyltrimethyl ammonium hydrochloride (ACTA) to confer a positive charge to the nanoparticle surfaces that facilitated nanosensor delivery to yeast cells, negating the need to use stress inducing techniques. The results showed that under glucose-starved conditions the intracellular pH of yeast population (n ≈ 200) was 4.67 ± 0.15. Upon addition of D-(+)-glucose (10 mM), this pH value decreased to pH 3.86 ± 0.13 over a period of 10 minutes followed by a gradual rise to a maximal pH of 5.21 ± 0.26, 25 minutes after glucose addition. 45 minutes after the addition of glucose, the intracellular pH of yeast cells returned to that of the glucose starved conditions. This study advances our understanding of the interplay between glucose metabolism and pH regulation in yeast cells, and indicates that the intracellular pH homestasis in yeast is highly regulated and demonstrates the utility of nanosensors for real-time intracellular pH measurements.

Introduction

Saccharomyces cerevisiae (yeast) is an eukaryotic unicellular model micro-organism that enables investigation of biological and metabolic processes[1]. For example, this model was used to elucidate the fundamental mechanisms of cell autophagy by Yoshinori Ohsumi, who was awarded the Noble Prize in medicine for his discoveries[2]. His investigations showed that the sophisticated cellular machinery in yeast is also used in human cells, paving the way towards understanding the fundamental physiological processes[3].

The intracellular pH of yeast is a key parameter that influences a number of biochemical processes, including survival, apoptosis, starvation, enzyme activation and ion transportation, which can also be used as indirect marker to monitor intracellular and metabolic processes[4]. During glucose metabolism, yeast cells exhibit transient changes in their intracellular pH, however, the mechanism of this process is yet to be confirmed[5-7]. Denhollander *et al.* have shown that changes in the intracellular pH of yeast during glucose metabolism are due to fluctuations in the carbon dioxide concentration, produced during glycolysis[8]. In contrast, it has been hypothesised that the intracellular pH of yeast is regulated by two different proton pumps, vacuolar H^+-ATPase (V-H^+ATPase) and plasma-membrane H^+-ATPase (P-H^+ATPase); activation of these ATPase pumps is highly dependent on glucose and ATP concentration[9, 10]. More recently, it has been reported that neither of these suggested mechanisms, fluctuations in carbon dioxide concentration or proton pump systems, is sufficient to explain the intracellular pH regulation of yeast during glucose metabolism[11]. This reflects the complexity of pH regulation in yeast and indicates that to understand the underlying mechanism of this process, further investigations and tools are required.

Methods and tools that have been used to investigate intracellular pH of yeast include:^{31}P nuclear magnetic resonance spectroscopy[12,13], pH-sensitive fluorophores[6,14-16], green fluorescent protein[17] and investigation of the distribution of labelled weak acids[18, 19]. However, these methods cannot be applied for longer

[a]School of Pharmacy, Boots Science Building, University of Nottingham, Nottingham, NG7 2RD, UK
[b]School of Life Sciences, University of Nottingham, Nottingham, NG7 2RD, UK
[c]Bioenergy and Brewing Science, School of Biosciences, Sutton Bonington Campus, University of Nottingham, Sutton, Leicestershire, LE12 5RD, UK,
[d]Current Address: Clinical and Experimental Sciences, Faculty of Medicine, Southampton General Hospital, University of Southampton, Southampton, SO16 6YD, UK and Anti-Doping Laboratory, Aspire Academy, Doha, Qatar
[e]Current Address: Vice-Chancellor's Department, University of York, Heslington, York, YO10 5DD, UK
*Address correspondence to: jon.aylott@nottingham.ac.uk; Fax: +44 (0) 115 9515102
†Authors contributed equally to this work.
‡ Electronic supplementary information (ESI) available: Further details regarding nanosensor characterisation (hydrodynamic diameters and surface charge) yeast incubated with unmodified nanosensor and using the hyperosmotic sodium chloride method for nanosensor delivery, optimisation of yeast growth time and incubation time, study of nanosensor toxicity and the pH colour heat maps for yeast cells for real-time pH measurements. The supplementary video shows processed data for the super-resolution structured illumination fluorescence microscopy imaging.

term or real-time measurements due to signal fluctuations and difficulty of *in-vivo* probe calibration. Furthermore, previously reported studies have also been unable to spatially resolve the pH differences amongst individual yeast cells, as it is thought that each yeast cell regulates its own independent pH[4]. Therefore utility of an effective sub-cellular probe, such as ratiometric fluorescent pH-sensitive nanosensors,[20] which permit real-time intracellular measurements, will enhance understanding of the fundamental mechanism of pH regulation in this model organism[21].

In this article we describe the utility of ratiometric fluorescent pH-sensitive nanosensors for the real-time measurement of the intracellular pH of yeast during glucose metabolism. Primarily, ratiometric fluorescent pH-sensitive nanosensors, with an extended dynamic pH range, were synthesised. In addition, an optimised protocol for nanosensor delivery that provided maximal cellular uptake and minimal toxicity was developed. Secondly, nanosensor localisation in yeast cells was investigated using super-resolution structured illumination fluorescence microscopy to confirm that nanosensors were successfully delivered. Finally, the real-time changes in the intracellular pH of yeast cells loaded with the pH-sensitive nanosensors were investigated in the presence of a glucose challenge.

Results and discussion

Nanosensor synthesis & characterisation

Ratiometric, fluorescent, pH-sensitive nanosensors with an extended dynamic pH range were synthesised as previously reported by Chauhan *et al.*[22]. This protocol produces pH-sensitive nanosensors consisting of an inert polyacrylamide nanoparticle matrix covalently linked to two pH-sensitive fluorophores, Oregon Green (OG) and 5(6)carboxyfluorescein (FAM), and a pH-insensitive reference fluorophore, 5(6)carboxytetramethylrhodamine (TAMRA). The synthesised nanosensors were characterised for their hydrodynamic diameters which centred at ~40 nm, with a narrow size distribution, and surface charge of 2.26 ± 3.7 mV (Figure S1 and S2, respectively). Nanosensor calibration was performed in citric acid monohydrate/sodium dibasic phosphate buffer solutions (pH 3.0 to 8.5). Combination of OG and FAM in a 1:1 ratio, within a single nanoparticle matrix, enables pH measurements over an extended dynamic range from pH 3.5 to 7.5, Figure S3[22, 23]. This broad pH measurement range can be utilised to make accurate measurements from diverse microenvironments, such as intracellular organelles.

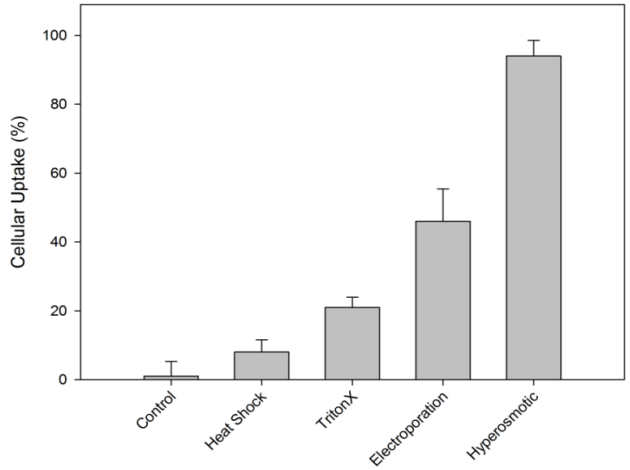

Figure 1: The effect of stress inducing techniques on yeast cellular uptake (%) of unmodified polyacrylamide pH-sensitive nanosensors that a surface charge of 2.26 ± 3.7 mV (Fig S1 †).

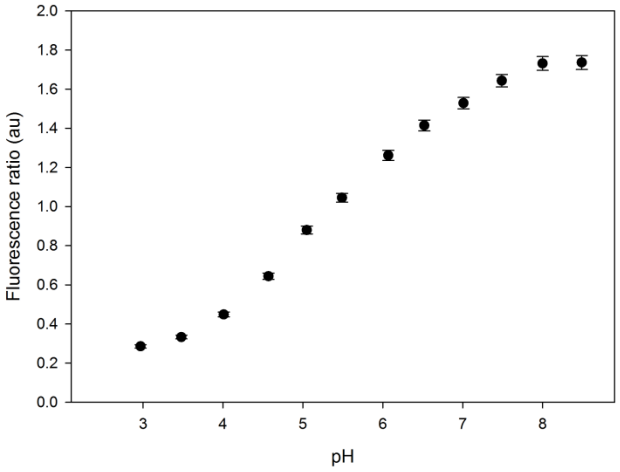

Figure 2. Ratiometric fluorescence calibration curve for the synthesised positively-charged pH-sensitive nanosensors, consisting of polyacrylamide nanoparticle matrix covalently linked to two pH-sensitive fluorophores (OG and FAM) and a reference fluorophore (TAMRA). Calibration curve was conducted on fluorescence microscope prior to intracellular pH measurements (error = standard deviation, n=3). See ‡ESI for emission and calibration curves for nanosensors recorded using fluorescence spectrophotometry, Figure S3.

Nanosensor delivery

The first challenge in this study was to deliver nanosensors to yeast cells with minimal cellular perturbation, so that any pH measurement made reflects their innate metabolic state. Initial efforts were directed at delivering the synthesised polyacrylamide nanosensors that had surface charge of 2.26 ± 3.7 mV. However, this proved to be ineffective (Figure S4) due to the yeast cell wall, an inherit part of yeast structure, which limits nanosensor delivery[24]. Previous reports have shown that stress inducing methods such as heat-shock[25], Triton-X/Amphotericin-B treatment[15], electroporation[26, 27] and hyperosmotic sodium chloride treatment[28] can improve particle or molecule delivery to yeast cells *via* permeabilization of the yeast cell wall and membrane. Poulsen *et al.* have reported that polyacrylamide-based nanosensors delivered to ≥ 50 % of yeast cells in a population is sufficient for analysis due to the challenges associated with traversing the yeast cell wall[27]. In this study, we investigated the transfection efficiency of a range of stress inducing techniques for the delivery of unmodified polyacrylamide nanosensors (zeta potential = 2.26 ± 3.7 mV), by measuring the percentage of cellular uptake (Figure 1). The results showed that hyperosmotic sodium chloride solution treatment was the most effective technique for nanosensor delivery with a cellular uptake of 94 ± 5 %. However, when these treated yeast cells were investigated further, morphological change to yeast cell structure had occurred (Figure S5). Therefore, this method was excluded from further study. In comparison, the widely-used technique of electroporation yielded a cellular uptake of 46 ± 9 %, in agreement with the 50 % cellular uptake that reported by Poulsen *et al.* Whilst the methods of Triton-X/Amphotricin-B and heat shock exhibited low cellular uptake of 21± 3 % and 8 ± 4 %, respectively. Due to the potential effects of stress inducing techniques on cellular viability and morphology, all these attempted stress inducing methods were not further utilised.

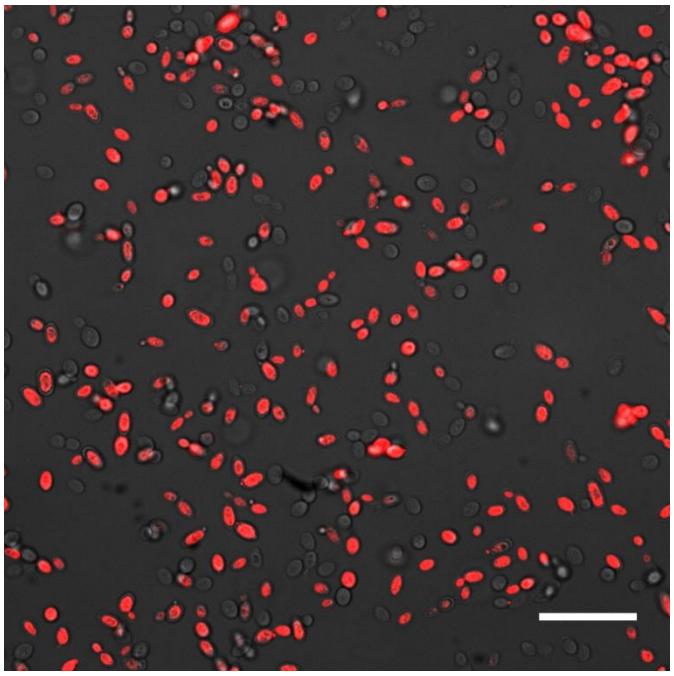

Figure 3. Representative fluorescent image of yeast cells, loaded with the positively-charged polyacrylamide nanosensors (surface charge of 17.5 ± 3.3 mV). The image was taken in the red channel (TAMRA) and shows that a cellular uptake of ~63% could be achieved *via* surface modification of nanosensors with a positively-charged functional group. Scale bar = 50 µm.

Alternate reports describing methods to augment nanoparticle delivery have shown that modification of nanoparticle surfaces with a positively-charged moiety can lead to enhanced cellular uptake[29-31]. Therefore, an acrylamide monomer, acrylamidopropyltrimethyl ammonium hydrochloride (ACTA)[32], was incorporated into the nanosensor matrix to produce positively-charged polyacrylamide pH-sensitive nanosensors of ~40 nm diameter that had a zeta potential of 17.5 ± 3.3 mV (Figure S1 and S2, respectively). These ACTA functionalised nanosensors produced a characteristic pH calibration curve when measured on a fluorescence spectrophotometer (Figure S3). When compared to unmodified nanosensors the calibration curve exhibited a shift to higher pH values. Further, the ACTA positively charged nanosensors were calibrated on a fluorescence microscope prior to analysis when incubated in yeast cells (Figure 2). Incubation of these positively-charged nanosensors with yeast yielded an improved cellular uptake to 63 ± 9 % by optimising the experimental parameters of yeast growth time (16-18 hours) and incubation time (4 hours), Figure S6 and S7 respectively. In addition, yeast cells loaded with positively-charged polyacrylamide nanosensors were intact and absent of any signs of morphological change, Figure 3. As a result, this optimised method for nanosensor delivery (ACTA functionalised nanoparticles, growth time of 16-18 hours, 4 hour incubation) was taken forward for further experimentation.

Cellular uptake & toxicity

In order to attain the maximal signal to noise, there is a trade-off between high signal and high nanosensor concentration, which could affect cell viability. In this study, we investigated the percentage of cellular uptake using a range of concentrations of positively-charged nanosensors, incubated with yeast cells, using

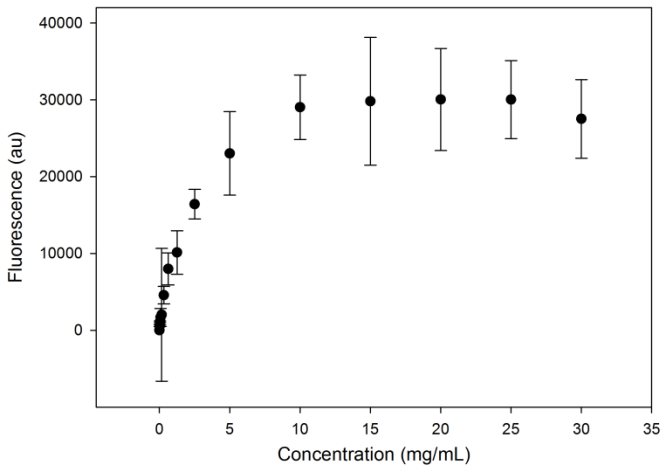

Figure 4. Cellular uptake study of yeast cells incubated with different concentrations (20 µg/mL-30 mg/mL) of positively-charged polyacrylamide nanosensors. Fluorescence intensity of TAMRA was recorded on a plate reader (λex = 545 nm & λem=575 nm) and was used as an indicator to determine cellular uptake.

the optimised nanosensor delivery protocol. The results showed that maximum cellular uptake (~63 %) was achieved at a nanosensor concentration of 10 mg/mL, Figure 4. Further, the toxicity of increasing nanosensor concentrations to yeast cells was investigated by quantifying colony forming units (CFUs)[30]. The CFUs results showed that the number of colonies produced from yeast, incubated with positively-charged nanosensors, was comparable to the negative control, yeast without nanosensors, up to a concentration of 25 mg/mL. Hereafter increasing nanosensor concentration reduced cellular viability (Figure S8).

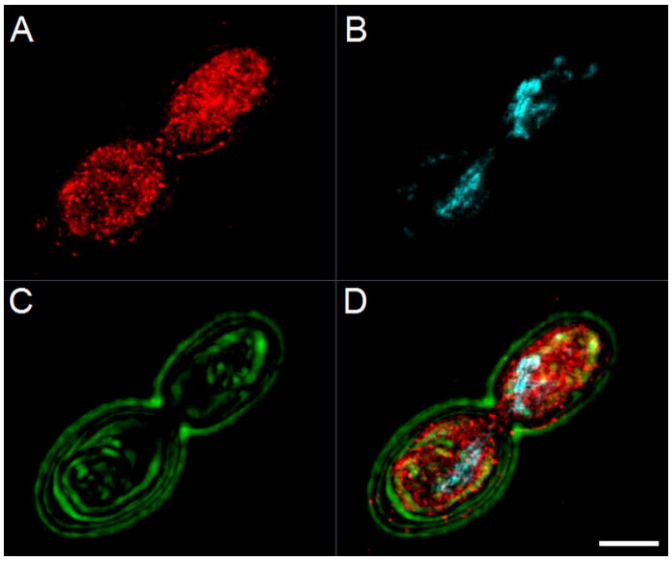

Figure 5. Super resolution structured illumination microscopy images of yeast cells loaded with (A) positively-charged, TAMRA-labelled, nanoparticles (red channel), (B) yeast stained with Hoechst 3334 (blue channel) to visualise the nucleus and nucleic acid. (C) False colour brightfield microscopy was used to determine the location of the cell wall and membrane (green channel). (C) Merged SIM image shows nanoparticles were evenly distributed inside the yeast cells and absent from the yeast nucleus. Scale bar = 2 µm.

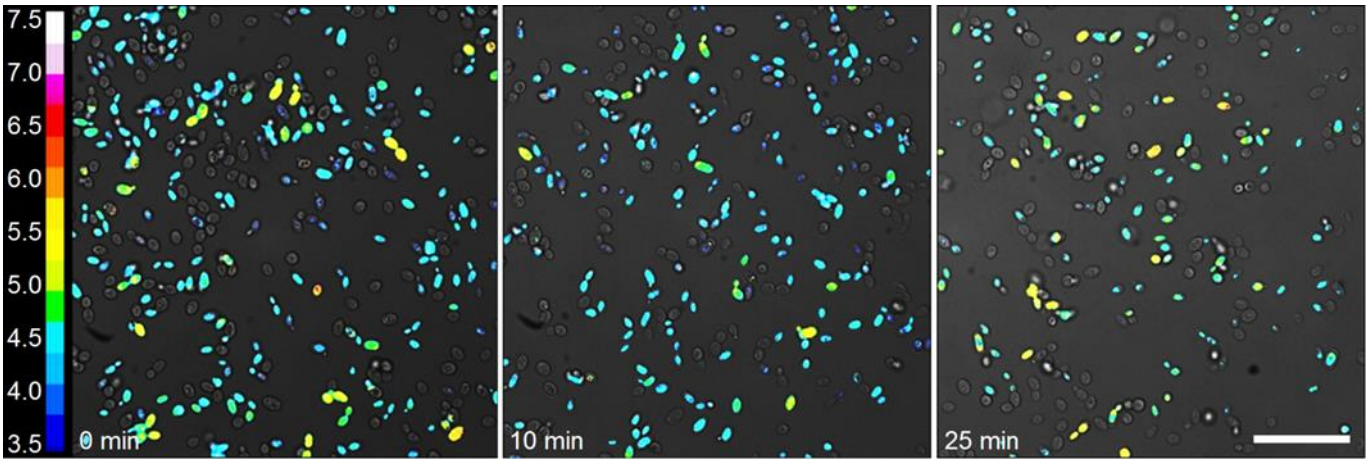

Figure 6. The false colour heat map images of yeast cells loaded with positively-charged pH-sensitive nanosensors at selected time points prior to glucose addition (0 min) for glucose-starved yeast cells, 10 minutes (10 min) and 25 minutes (25 min) after glucose addition to glucose-starved yeast. Scale bar = 50 µm.

Nanosensor localisation

To determine the yeast sub-cellular micro environments from which pH measurement would be made, super-resolution fluorescence structured illumination microscopy (SIM) was used to visualise the location of nanoparticles in the yeast cells (Figure 5). The cells were incubated with positively-charged, TAMRA-labelled (red channel) polyacrylamide nanoparticles (characterised to show the same size and surface charge as nanosensors) and cells were stained with Hoechst 3334 (blue channel) to determine the location of the nucleic acid and yeast nucleus.

The cell wall and cell membrane were identified by false colour brightfield imaging (green channel). Figure 5 and Supplementary Movie 1 indicate that positively-charged nanoparticles were distributed in the yeast intracellular microenvironment. Furthermore, the nucleus, highlighted by Hoechst 3334 nucleic acid staining, contained some fluorescent signals in the red channel, which suggest that nanoparticles are also to some extent able to penetrate the nuclear membrane. Additionally, nanoparticles were observed at the edge of the cells, attached to the cell wall, suggesting that some nanoparticles were trapped within these regions prior to traversing the yeast cellular wall and membrane. Taken together the high resolution imaging confirms nanoparticles were inside the yeast and well distributed throughout the cell and can be used for intracellular pH measurements.

Measurement of the intracellular pH of yeast during glucose metabolism

To detect the intracellular pH of yeast during glucose metabolism, yeast cells loaded with positively-charged pH-sensitive polyacrylamide nanosensors were visualised and imaged using fluorescence microscopy in the starved state and after addition of D-(+)-glucose (10 mM). The intracellular pH of each individual yeast cell was detected and used to calculate the mean intracellular pH of yeast cell population, under the field of view, to establish the real-time pH response of yeast during glucose metabolism. The results showed that in the absence of glucose, each yeast cell exhibited an independent intracellular pH, while the intracellular pH of yeast population ($n \approx 200$) was 4.67 ± 0.15, Figure 6 (0 min). Upon addition of glucose, the mean intracellular pH of yeast population decreased to pH 4.56 ± 0.09 (1 minute) and to a minimum of pH 3.86 ± 0.13, 10 minutes after glucose addition (Figure 7).

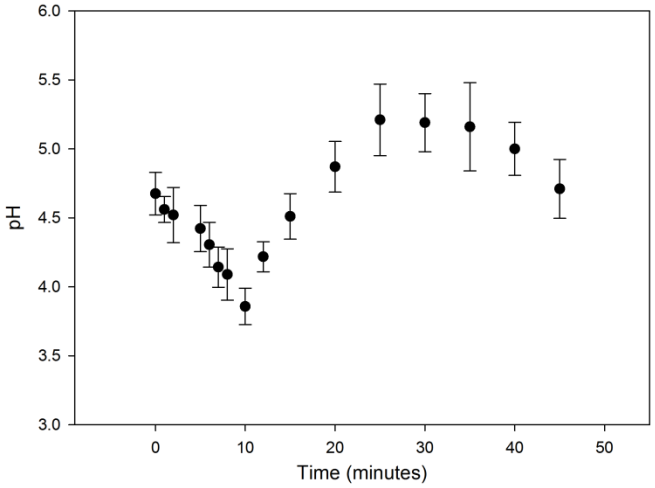

Figure 7. The real-time intracellular pH response of yeast cell population in the starved state and after addition of D-(+)-glucose (10 mM, at time 0 minutes) for a period of time up to 45 minutes.

Hereafter, the intracellular pH of the yeast increased to a maximum pH 5.21 ± 0.26, 25 minutes after glucose addition. This elevated pH was sustained for a further 15 minutes before returning back to the starved pH conditions (pH 4.71 ± 0.22) 45 minutes post glucose addition (Figure S9).

Our findings complement research conducted by Ozalp *et al.*[33] who studied the intracellular ATP concentrations during glucose metabolism, using ATP-sensitive nanosensors. Their results have shown that upon glucose addition to glucose-starved yeast cells, ATP concentration initially increased (~1-2 minutes) and then gradually decreased, due to ATP consumption and ATPase activity. Subsequently the ATP concentration recovered to the initial level (glucose-starved state), 20 minutes after glucose addition, which declined after 45 minutes post-glucose addition[33]. Bearing Ozalp *et al.* observations in mind, we postulate that pH fluctuations observed in our experiments are indicative of glucose metabolism that produces ATP which is used to activate the ATPase proton pumps. This process is highly regulated and dependent on glucose such that after glucose consumption the cell returns back to glucose starved states.

Conclusions

In summary, we have demonstrated how ratiometric fluorescent pH-sensitive nanosensors can be applied to yeast cells and used to detect real-time intracellular pH changes in the presence of a glucose challenge. Through nanosensor surface modification with a positively-charged functional group, we were able to outperform stress inducing techniques, including heat shock, Triton-X, electroporation and hyperosmotic treatment to deliver nanosensors to yeast. Nanosensors were delivered to yeast cells in high amounts, whilst limiting toxicity and perturbations to yeast morphology. Under starved conditions yeast cells, loaded with pH-sensitive nanosensors, reported an intracellular pH of 4.67 ± 0.15. However, upon addition of glucose the pH initially decreased to 3.86 ± 0.13 followed by a rise to pH 5.21 ± 0.26, higher than the starved glucose conditions. The intracellular pH returned to the starved state conditions after a period of 45 minutes. This pH oscillation could be attributed to activation of the ATPase proton pumps of yeast cells by ATP molecules produced during glucose metabolism. These results indicate that the intracellular pH homeostasis of yeast is highly regulated and dependent on glucose. Our findings provide a mechanistic insight into the regulatory role of pH during glucose metabolism in yeast and will find broad utility of using nanosensors in analytical and biological applications, including real-time investigations of intracellular and metabolic processes.

Experimental

Materials

Oregon Green 488 carboxylic acid succinimidylester-5-isomer (OG), 5-(6)-carboxyfluorescein succinimidylester (FAM) and 5-(6)-carboxytetramethylrhodamine succinimidylester (TAMRA) were obtained from Invitrogen, USA. Acrylamide 99% minimum, N, N' methylenebis(acrylamide) (bisacrylamide), polyoxyethylene(4)lauryl ether (Brij 30®) were purchased from Fluka Analytical, UK. N-(3-aminopropyl)methacrylamide hydrochloride (APMA) and 3-acrylamidopropyltrimethyl ammonium hydrochloride (ACTA) were obtained from Polysciences Inc, Germany. Dioctylsulfosuccinate sodium (AOT), ammonium persulphate (APS), N,N,N,N-tetramethylethylenediamine (TEMED), hexane, sodium borate, ethanol absolute (99.5%) and phosphate buffer saline (PBS) were obtained from Fisher Scientific, UK. Unless otherwise mentioned, all the chemicals that used throughout this study were of analytical grade.

Nanosensor fabrication [22, 32]

Prior to nanosensor synthesis, the succinimidyl ester derivative of each fluorophore was conjugated separately to APMA to produce fluorophore-APMA conjugates that were further used to covalently bind nanoparticle matrix. Briefly, 5 mg of APMA was dissolved into 2.5 mL of sodium borate buffer (50 mM, pH 9.5) and then 200 µL of this solution was added to 1 mg of the succinimidyl ester derivative of each fluorophore (OG, FAM and TAMRA), prepared in separate vials. The reaction mixtures were stirred for at least 24 hours in the dark at room temperature and stored at 4° C until further use.

To synthesis positively-charged, ratiometric, fluorescent, pH-sensitive nanosensors, 1.590 g of AOT and 3.080 g of Brij 30® were mixed together into a 250 mL round bottom flask, and purged under argon for 15 minutes followed by addition of 42 mL of deoxygenated hexane that had previously been purged with argon for at least 30 minutes. The flask was sealed under an inert argon atmosphere using a balloon with continuous stirring. Following this, 513.0 mg of acrylamide, 152.0 mg of bisacrylamide and 119 µL of ACTA (75 % w/v) were dissolved into 1.5 mL water and then added into the sealed flask containing the surfactants and hexane mixture using a syringe. APMA-fluorophore conjugates, purged with argon, were then added using 15 µL of OG-APMA, 15 µL of FAM-APMA and 60 µL of TAMRA-APMA, by a syringe. Finally, 30 µL of APS (10% w/v) and 15 µL of TEMED were added and the stirring was continued for 2 hours in the dark under a sealed argon atmosphere. The reaction was halted by removing the stopper and exposing the flask content to air. To isolate the synthesised nanosensors, hexane was removed by rotary evaporation at 30° C and then 30 mL of ethanol was added to the flask content. The mixture was transferred into a 50 mL falcon tube and centrifuged for 10 minutes at 6000 rpm. Washing with 30 mL ethanol was performed 5 times and in the last wash, 10 mL of ethanol was added and removed by rotary evaporation at 30 °C. The dried nanosensors were stored at -20 °C until further use.

Yeast strain and growth conditions

The yeast strain used in this study was *Saccharomyces cerevisiae* NCYC2592. The cells were incubated, with shaking at 28 °C and 150 rpm, into a 250-mL Erlenmeyer flask containing 50 mL of minimal yeast nitrogen base dextrose (YNBD) medium with 6.7 g/L yeast nitrogen base without amino acids (Difco®) and 20 g/L of glucose, pH 5.5. The medium was inoculated by a single colony, taken from yeast culture that had previously cultivated on YNBD-agar. The cells were harvested after 16-18 hours where the optical density (OD_{600}), measured by a spectrophotometer at 600 nm, was 1.0 ± 0.2.

Cellular uptake study

Yeast cells were grown in YNBD medium (50 mL) for 16-18 hours, OD_{600} of 1 mL of cell suspension was measured (1.0 ± 0.2) and followed by centrifugation at 5000 rpm for 10 minutes at 4 °C. The cell pellets were resuspended in 1 mL of phosphate buffer, pH 5.5, using a vortex mixer and then centrifuged at 5000 rpm for further 10 minutes at 4 °C. This washing step was repeated three times with phosphate buffer followed by the incubation of 100 µL of cell suspensions with a range of concentrations (20 µg/mL-30 mg/mL) of positively-charged nanosensors, prepared by serial dilution using phosphate buffer, pH 5.5. The yeast cells were then incubated with these nanosensors for 4 hours followed by centrifugation and washing for at least five times using 1 mL of phosphate buffer, pH 5.5. Following this, 100 µL of the yeast, incubated with positively-charged nanosensors, were transferred into 96-black well plate block (Costar 96 well plate, from Bio-Rad, UK) and the relative fluorescence unit (RFU) of TAMRA were recorded using a Tecan Spark M10 plate reader at 575 nm after excitation at 545 nm and compared to blank yeast sample.

Toxicity study

The same procedure that was described above for the cellular uptake study was followed. After yeast incubation with positively-charged nanosensors (20 µg/mL-30 mg/mL) and performing the washing steps; 10^5 times serial dilution of the cell suspensions were made using phosphate buffer for each corresponding nanosensor concentration. Following this, 100 µL of the diluted cell suspensions were spread on YNBD-agar in Petri dishes. The Petri dishes, containing the yeast cells, were incubated for 48 hours at 28 °C and the number of the produced colonies, corresponding to each yeast sample that incubated previously with positively-charged

nanosensors was counted and compared to the number of colonies of the control sample, where no nanosensors were incubated with yeast and treated similarly.

Incubation time

100 µL of yeast cell suspensions, prepared as in the cellular uptake study, were incubated with 15 mg/mL of positively-charged nanosensors for different time intervals ranging from 0-24 hours followed by centrifugation and 6 washes with phosphate buffer. The fluorescence intensity of TAMRA was measured by spectrofluorimetry using excitation and emission wavelengths of 545 nm and 577 nm, respectively.

Super-resolution structured illumination fluorescence microscopy (SIM*)*

Yeast cells were loaded with positively-charged, TAMRA-labelled polyacrylamide nanoparticles, with a diameter of ~40 nm, using the optimised nanosensor delivery protocol (16-18 hour growth time, 4 hour incubation). Incubated yeast cells were permeabilized with Triton-X, 0.1 % in PBS for 10 minutes. Samples were washed twice with PBS and incubated overnight with Hoechst 33342, DNA dye. After a further two washes with PBS yeast cells were fixed with 4% paraformaldehyde (PFA), for 10 minutes and washed again twice washed twice with PBS after fixation. The cell pellet was re-suspended in Prolong Gold mounting media and mounted with high precision coverslips (Zeiss®, thickness no. 1.5H, 474030-9000-000). SIM imaging was performed using structured illumination module on Zeiss Elyra PS.1 microscope. Prolong gold mounted samples were scanned at 27°C, using Zeiss Immersol® 518F/30°C), with Plan-Apochromat 63x/1.4 Oil DIC M27 objective. TAMRA- labelled nanoparticles were detected with BP 570-620 + LP 750, and DNA staining with BP 420-480 + LP 750, respectively. A third SIM imaging track was set up with transmitted light; brightfield images were recorded using the halogen lamp, and no laser was assigned, using the BP 495-550 + LP 750 filter. TetraSpec™ Microspheres (0.1 µm) were used to asses and correct for channel alignment (Thermo Fisher cat. no. T7279). Image processing was done using Zeiss Zen Black, SIM module. Filtering was set to the following values: red channel Noise_Filter-4.6475, Auto_Noise_Filter on, Sectioning: 98, 83, 83, blue channel Noise_Filter-4.2217, Auto_Noise_Filter on, Sectioning: 99, 83, 83, brightfieldNoise_Filter -1, Auto_Noise_Filter off, Sectioning: 98, 83, 83. Note we used lowest value for the bright field channel, in order to remove honeycomb-like artefacts. Since the cell wall is a high contrast object, the brightfield processed image we visualized in the 3D rendered images, by setting the threshold to 71.2 and assigning green colour to it (see Figure 5 & Supplementary Movie 1).

Nanosensors calibration

Positively-charged nanosensors (1 mg/mL) were suspended in citric acid monohydrate/sodium dibasic phosphate buffer solutions, prepared with different pH values from pH 3.0 to 8.5. Nanosensors, suspended in each pH value, were transferred into glass dishes and calibration images were taken using the fluorescence microscope in the merged channels (green, red channels and brightfield mode). The microscope was focused using a scratch inside the glass bottom of each dish and subsequently moved away from the scratch to acquire the images. Images were taken from three different areas around the centre of the scratch, background-corrected ratiometric images were established by using MATLAB® software and were used to construct the calibration curve as reported [22].

Measurement of the intracellular pH of yeast cells

After growing yeast for 16-18 hours, yeast cells were collected as previously described and suspended in phosphate buffer. The glucose starvation process was initiated by incubation of 100 µL of cell suspension, with positively-charged nanosensors (15 mg/mL) for 4 hours in phosphate buffer, pH 5.5, without any glucose or nutrients. The incubated cell suspensions were centrifuged and washed, several times. Following this, 5 µL of glucose-starved yeast suspensions was transferred to standard glass coverslips and cell imaging commenced. Images were immediately taken for the cells using the fluorescence microscope in the merged channels (green, red and brightfield). The nanosensor calibration was performed under the same optical parameters and experimental conditions. Once the images of glucose-starved cells were acquired, 10 mM of D-(+)-glucose was added to the cell suspensions and images were continuously taken at successive time intervals which ranged from 1 minute to up to 45 minutes. The time lapse between each image was set to 1 minute within the first 10 minutes and then every 5 minutes during the experiment duration.

Image acquisition and data analysis

Automated images acquisition and data analysis of nanosensor calibration and yeast cells were performed using a previously reported protocol, established by our research group [22]. Ratiometric fluorescent images and background images (buffer without nanosensors) were acquired in all channels (red, green and brightfield) for each corresponding pH value. Images were taken using a 40x objective lens (Nickon, Plan Fluor 0.75) in the green channels for OG and FAM (excitation at 490 nm, fluorescence at 525 nm), red channels for TAMRA (excitation at 550 nm, fluorescence at 580 nm) and brightfield mode. The size of all images was set to 1024×1024 pixels. Background-corrected ratiometric images were generated automatically using MATLAB® software after subtraction of the background images (blank samples containing buffers with no nanosensors) from the corresponding ratiometric fluorescent images. The calibration curve of nanosensors was constructed as a function between the mean of the pixel ratios of three background-corrected ratiometric images (green/red) of the nanosensors versus the corresponding pH value. A similar procedure was followed to generate the background-corrected ratiometric images for the yeast cells. Calculations of the intracellular pH of the cells were performed using ImageJ® software by selection of a pixel-wise area of the background-corrected ratiometric images of the cells-containing nanosensors. The results were matched with the calibration curve data. Additionally, ImageJ® software was used to construct the false colour heat map pH images. To measure the intracellular pH, the areas of the fluorescent cells (yeast-containing nanosensors) in the background-corrected ratiometric images were selected and the pixel intensities of the selected areas were calculated using ImageJ®. The fitting equation of the calibration curve was applied to measure the pH of the imaged cells using MATLAB® and ImageJ®[22, 32].

Acknowledgements

We would like to thank Dr Chris Powell and Mr Abdelrahman Saleh Zaky at the Bioenergy and Brewing Sciences, School of Bioscience, University of Nottingham for their support and co-operation during this work and for kindly providing the yeast cells and the growth media that were used through this work. Microscopy was performed at the Multidisciplinary Super Resolution Microscopy

Facility at Nottingham, funded by BBSRC BB/L013827/1, and run by the School of Life Sciences Imaging (SLIM), of Nottingham University. This research was funded by the University of Nottingham and the Islamic Development Bank.

References

1. G. M. Walker, *Yeast Physiology and Biotechnology*, John Wiley & Sons Ltd, West Sussex, UK, 1998.
2. The Noble Prize Organisation, https://www.nobelprize.org/nobel_prizes/medicine/laureates/2016/press.html?ctkey=autophagy).
3. T. Noda and Y. Ohsumi, *J Biol Chem*, 1998, **273**, 3963-3966.
4. R. Orij, S. Brul and G. J. Smits, *Biochim Biophys Acta*, 2011, **1810**, 933-944.
5. R. S. Haworth and L. Fliegel, *Mol Cell Biochem*, 1993, **124**, 131-140.
6. P. Breeuwer and T. Abee, *J Microbiol Methods*, 2000, **39**, 253-264.
7. S. Bond and M. Forgac, *J Biol Chem*, 2008, **283**, 36513-36521.
8. J. A. Denhollander, K. Ugurbil, T. R. Brown and R. G. Shulman, *Biochemistry*, 1981, **20**, 5871-5880.
9. G. A. Martinez-Munoz and P. Kane, *J Biol Chem*, 2008, **283**, 20309-20319.
10. A. B. Mason, T. B. Kardos and B. C. Monk, *Biochim Biophys Acta*, 1998, **1372**, 261-271.
11. M. T. Kresnowati, C. M. Suarez-Mendez, W. A. van Winden, W. M. van Gulik and J. J. Heijnen, *Metab Eng*, 2008, **10**, 39-54.
12. G. Navon, R. G. Shulman, T. Yamane, T. R. Eccleshall, K. B. Lam, J. J. Baronofsky and J. Marmur, *Biochemistry*, 1979, **18**, 4487-4499.
13. R. J. Gillies, K. Ugurbil, J. A. den Hollander and R. G. Shulman, *Proc Natl Acad Sci U S A*, 1981, **78**, 2125-2129.
14. C. Weigert, F. Steffler, T. Kurz, T. H. Shellhammer and F. J. Methner, *Appl Environ Microbiol*, 2009, **75**, 5615-5620.
15. M. Valli, M. Sauer, P. Branduardi, N. Borth, D. Porro and D. Mattanovich, *Appl Environ Microbiol*, 2005, **71**, 1515-1521.
16. M. Valkonen, D. Mojzita, M. Penttila and M. Bencina, *Appl Environ Microbiol*, 2013, **79**, 7179-7187.
17. I. I. Kunze, G. Hensel, K. Adler, J. Bernard, B. Neubohn, C. Nilsson, R. Stoltenburg, S. D. Kohlwein and G. Kunze, *Biochim Biophys Acta*, 1999, **1410**, 287-298.
18. M. T. Kresnowati, C. Suarez-Mendez, M. K. Groothuizen, W. A. van Winden and J. J. Heijnen, *Biotechnol Bioeng*, 2007, **97**, 86-98.
19. L. U. Guldfeldt and N. Arneborg, *Appl Environ Microbiol*, 1998, **64**, 530-534.
20. R. V. Benjaminsen, H. Sun, J. R. Henriksen, N. M. Christensen, K. Almdal and T. L. Andresen, *ACS Nano*, 2011, **5**, 5864-5873.
21. T. Vo-Dinh, *Nanotechnology in Biology and Medicine: Methods, Devices and Applications*, Taylor and Francis Group, CRC Press, New york, USA, 2007.
22. V. M. Chauhan, G. Orsi, A. Brown, D. I. Pritchard and J. W. Aylott, *ACS Nano*, 2013, **7**, 5577-5587.
23. V. M. Chauhan, G. R. Burnett and J. W. Aylott, *Analyst*, 2011, **136**, 1799-1801.
24. J. Ruiz-Herrer, *Fungal Cell Wall: Structure, Synthesis, and Assembly*, CRC Publisher, Florida, USA, Second Edition edn.
25. P. W. Piper, C. Ortiz-Calderon, C. Holyoak, P. Coote and M. Cole, *Cell Stress Chaperones*, 1997, **2**, 12-24.
26. M. P. Coogan, J. B. Court, V. L. Gray, A. J. Hayes, S. H. Lloyd, C. O. Millet, S. J. Pope and D. Lloyd, *Photochem Photobiol Sci*, 2010, **9**, 103-109.
27. A. K. Poulsen, A. Z. Andersen, J. C. Brasen, A. M. Scharff-Poulsen and L. F. Olsen, *Biochemistry*, 2008, **47**, 7477-7484.
28. Jumpei Miyazaki, Yuta Kuriyama, Akihisa Miyamoto, Hayato Tokumoto, Yasuhiro Konishi and a. T. Nomura, *Advanced Powder Technology*, 2014, **25**, 1394–1397.
29. C. He, Y. Hu, L. Yin, C. Tang and C. Yin, *Biomaterials*, 2010, **31**, 3657-3666.
30. T. Nomura, J. Miyazaki, A. Miyamoto, Y. Kuriyama, H. Tokumoto and Y. Konishi, *Environ Sci Technol*, 2013, **47**, 3417-3423.
31. R. R. Arvizo, O. R. Miranda, M. A. Thompson, C. M. Pabelick, R. Bhattacharya, J. D. Robertson, V. M. Rotello, Y. S. Prakash and P. Mukherjee, *Nano Lett*, 2010, **10**, 2543-2548.
32. A. Desai, PhD, University of Nottingham, 2014.
33. V. C. Ozalp, T. R. Pedersen, L. J. Nielsen and L. F. Olsen, *Journal of Biological Chemistry*, 2010, **285**, 37579-37588.